Journal of Alloys and Compounds 658 (2016) 875–879

Contents lists available at ScienceDirect

Journal of Alloys and Compounds

journal homepage: http://www.elsevier.com/locate/jalcom

Laser-assisted synthesis in Cu–Al–Ni system and some of its properties

I. Shishkovsky [a, b, *], I. Yadroitsev [b], Yu. Morozov [c]

[a] Lebedev Physical Institute (LPI) of Russian Academy of Sciences, Samara Branch, 443011 Samara, Russia
[b] Ecole Nationale d'Ingénieurs de Saint-Etienne, DIPI Lab, 58 Rue Jean Parot, 42023 Saint-Etienne, France
[c] Institute of Structural Macrokinetics and Materials Science, Russian Academy of Sciences, Academician Osipyan Str. 8, Chernogolovka, Moscow Region 142432, Russia

ARTICLE INFO

Article history:
Received 3 August 2015
Received in revised form
23 October 2015
Accepted 31 October 2015
Available online 10 November 2015

Keywords:
Selective laser sintering/melting (SLS/M)
Intermetallic phase synthesis
Shape memory effect (SME)

ABSTRACT

Conditions of intermetallic phase synthesis during layerwise selective laser sintering/melting in Cu–Al–Ni powdered system were explored. There to we used optical and scanning electron microscopy, EDX and XRD analysis for microstructure testing and intermetallide identification in porous 3D samples depending on the laser syntheses regimes. A high laser sintering ability of the prepared mixtures and shape memory effect in 3D samples by results of specific electrical resistance measurements were shown. Porosity of the laser-synthesized Al_7Cu_4Ni intermetallide led to a peak shifting by the temperature axis and the intervals of the A_s–A_f austenite transformation and M_s–M_f martensite transformation were 50 ÷ 80 °C and +25 ÷ −40 °C respectively.

1. Introduction

At first laser controlled self-propagated high-temperature syntheses (SHS) of perspective chemical compounds were realized [1]. By this time this scheme had been realized in dozens of reactionary powdered mixtures (see review [1]). It is known that intermetallic phases in Ni–Al [2–5] and Cu–Al–Ni [6,7] systems can be obtained in reactions of the laser syntheses. The interest to the phases and 3D parts based on these phases is explained by their shape memory effect (SME) [8–12]. In papers [9,13] it was supposed, that the materials and the SME could be used in medicine. Depending on the composition, structure and way of manufacturing the material, the temperature intervals of SME can deviate [13–15] from tabular data (Cu–Al–Ni, 14% wt. Al and 4% wt. Ni, −140 to 100 °C) owing to a reversible austenite – martensite transformation. Conventionally, Cu–Al–Ni shape memory alloys (SMA) are obtained either by melting of pure elements in an argon atmosphere with a high-speed quenching or by the SHS process [16–20]. Unfortunately, within the framework of these approaches the samples of simple shape could only be obtained, so searching of new methods for complex shape manufacturing of the SMA as well as techniques of obtaining SME are of interest.

Selective laser sintering/melting (SLS/M) process is the unique additive technology [1,2,4,5,7,21–23] allowing layerwise 3D samples fabricating out of powdered material on the basis of CAD data. Not less perspective is the fabricating of not just functional products, but artificial medical devices – the micro-electro – mechanical systems (MEMS) [1,23]: implants, fixing grips, drug delivery systems etc. by this technique.

In the present study, it was offered to synthesize intermetallides in the Cu–Al–Ni system by the method of overlapping SLS/M and SHS and determine some of their electro-mechanic properties, which is prospective for medical applications.

2. Experimental

All the reagents used in experiments were obtained from French chemical market and used as supplied. CuNi10 powder produced by TLS Technik GmbH and having the following composition (Cu – balance, Ni – 10%, Fe – 1–2%, Mn – 0.5–1%, C – 0.05%, Pb – 0.05%, Zn – 1% wt. max.) and aluminum powder graded Grenaille 350TL (Métaux & Chimie) were mixed in the ratio enabling to obtain a stoichiometric Cu–Al14%–Ni4% phase. The particle size distribution was studied by means of an optical granulomorphometer ALPAGA 500NANO which is a real-time optical sieving system, and the CALLISTO image analysis software (OCCHIO s.a.). The

* Corresponding author. Lebedev Physical Institute (LPI) of Russian Academy of Sciences, Samara Branch, 443011 Samara, Russia.
E-mail address: shiv@fian.smr.ru (I. Shishkovsky).

http://dx.doi.org/10.1016/j.jallcom.2015.10.299
0925-8388/

morphology structures of the raw powders are presented in Fig. 1(a, b). Most of the particles had high spherical shapes and smooth surface with a negligible quantity of satellites. The CuNi10 powder had average size of ~25 μm, apparent density 5.3 ± 0.01 g/cm^3, evident density 4.8 ± 0.06 g/cm^3, volume specific surface ~0.467 μm^{-1}. The Al powder had average size of ~30 μm, apparent density 1.85 ± 0.03 g/cm^3, evident density 2.7 ± 0.05 g/cm^3, volume specific surface ~0.102 μm^{-1}. The powder particles had mainly spherical surface and insignificant size dispersion that ensured a uniform distribution under layer-by-layer delivering in the SLS/M process.

Experiments were conducted in DIPI laboratory (ENISE, France) on the SLS/M setup – PM 100 (Phenix Systems). In the PM-100 the solid-state fiber ytterbium laser YLR-100 (IPG Photonics) is used, working in the cw regime on the wavelength of λ = 1.075 μm. Main features of PM 100 setup were the following: power $P = 50–70$ W, laser beam diameter 70 μm. Laser sintering/melting was carried out on the metallic platform, a minimum layer incrementation was about the powdered composition size, synthesis occurred in a protective gas (argon) environment. One and two-zone scanning strategies [8] were used with a hatch distance of *Sh* ~ 80 μm between passages and laser scan velocities of v = 120, 140, and 160 mm/s.

After etching, cross sections of the multi-layered SLM samples were subjected to the metallurgical analysis with the optical microscope (Olympus BX51, Japan) equipped with a digital camera. The phase composition of the synthesized structures was determined with X-ray diffraction (XRD) using a DRON-3 diffractometer in Cu-K_α radiation, JCPDS PDF data (PCPDFWIN ver. 2.02, release 1999) and the Crystallographica SearchMatch ver. 3.102 program. Morphology of the laser sintered/melted layers and 3D samples after the SLS/M was studied with a LEO 1450 scanning electron microscope (Carl Zeiss Company) equipped with an electron dispersion spectroscopy (EDS) (INCA Energy 300, Oxford Instruments).

Specific electrical resistivity (ER) ρ was accurately measured by four-probe potentiometric method (Fig. 2, [13]) within a temperature range from −150 °C up to +200 °C. Flat 2D monolayers with sizes 10 × 30 × d mm (where *d* is thickness of one separate monolayer, see Fig. 2) were synthesized in powder volume. The temperature range taken for the thermal cycling was much wider than one used for Cu–Ni–Al transformation. The reason for such measure is that, governed by some rules, temperature points in porous heterogeneous structures could be displaced [23]. An external heater and liquid nitrogen were employed to vary the temperature of the CuNiAl samples. The temperature was measured by Chromel–Alumel thermocouple. The laser welding and low-resistance solders were used to minimize measurement mistakes.

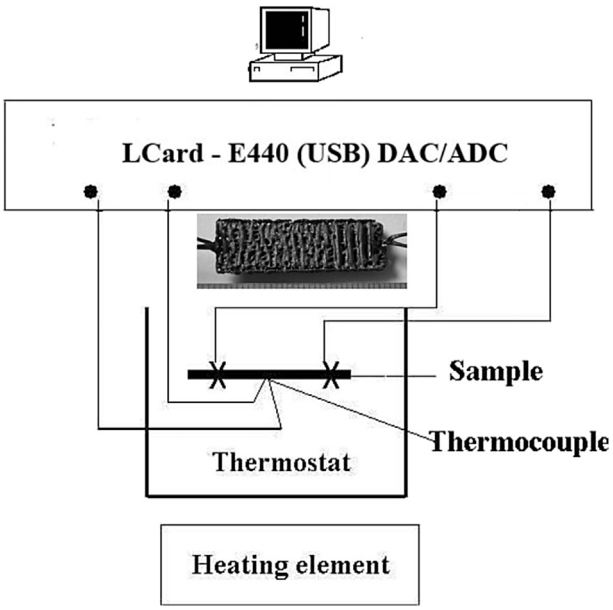

Fig. 2. Appearance of the 2D monolayer with laser welded electrodes and specific measurements of ER *vs.* temperature by four-probe potentiometric method.

The relative accuracy of the resistivity measurement was determined by the accuracy of the temperature measurement (relative accuracy of 0.1 °C) and was estimated to be within 10^{-4}.

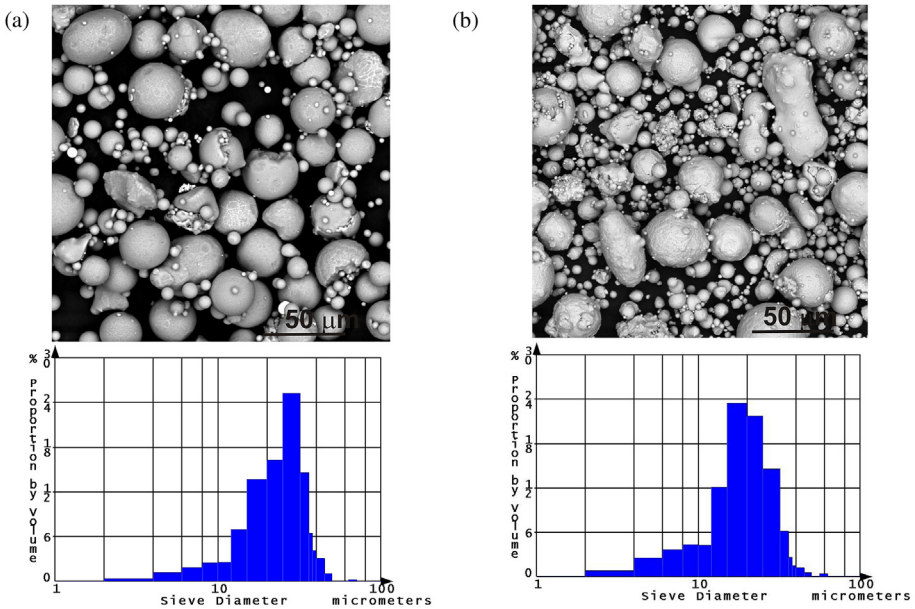

Fig. 1. Morphology view and particle size distributions of Al – a) and CuNi10 – b) powders.

The experimental data were digitized by Labview program on DAC/ADC (LCard Co, Moscow, RF).

3. Results and discussion

In accordance with the ternary phase diagram [17] we expected to obtain the following stable intermetallic phases of the Cu–Ni–Al system after a high-speed laser cooling: α + γ2/β + NiAl or α + β + γ2 phases. The experimental measurements of temperature in the volume of similar but binary Ni–Al/Ni–Ti powder mixtures during the SLS process, as well as the maximum temperature reachable in the reaction media and numerical simulations for the SHS + SLS processes were obtained by us earlier in studies described in papers [24–26].

Firstly, we defined the SLS/M conditions for separate monolayers on the metallic substrate and in the powder copiously filling the volume. The exterior view of a monolayer after the bulk SLS prepared for the following electrophysical testing is shown in Fig. 2 (insertion). The range of the layer thicknesses is presented in Fig. 3 and it fluctuates within the interval of 1.3–1.9 mm. The experimental optimization of the monolayer depth has similar dependence as results those obtained for Ni–Al and Ni–Ti powdered mixtures presented in Refs. [1,2,5].

However, after transition to the SLS/M on the metallic substrate this range shifted to the area of greater laser energy inputs. This is connected with more intensive heat dissipation under the SLS/M process on the metallic platform than in the powdered volume. The Fig. 4 shows one of the successful results of the layerwise SLM. Experimental estimated density of the 3D disk sample from Fig. 4 was 4.96 g/cm^3 (under 7.12 g/cm^3 for ingot CuAlNi SMA).

For clarification of element composition of the obtained microstructures and inclusions, the SEM with EDS microanalysis was carried out. Before analysis, we restricted into EDS data (Table 1) the element quantity (namely, oxygen and carbon) due to we have deal with porous structure on the surface of which a carbon dioxide was absorbed. High-resolution SEM results for the porous surface in electron backscattering mode are presented in Fig. 5 after the SLM. Fig. 5a is shown a common view of a porous structure after a high-speed laser remelting. As it is seen, the light gray color matrix stands for initial CuNi10 powder, however vastly depleted by nickel and enriched by aluminum (S3 and S4 area, Table 1). The "S1-All" index is written with such EDS data, in which information was collected from the whole of area of the corresponding figure. The EDS data (S1 row) is corresponding to the Al_7Cu_4Ni intermetallic phase (58.33/8.33/33.33%). Evidently, this is the result of the laser

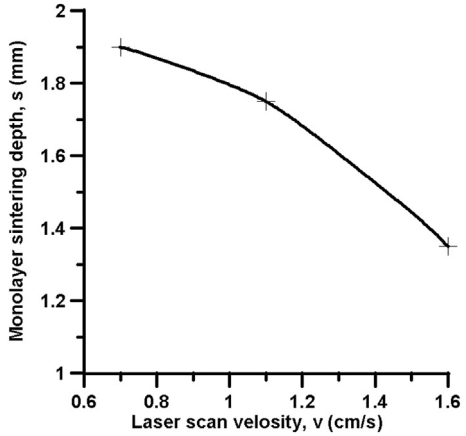

Fig. 3. Monolayer sintering depth *vs.* laser scan velocity. Laser power $P = 23.5$ W.

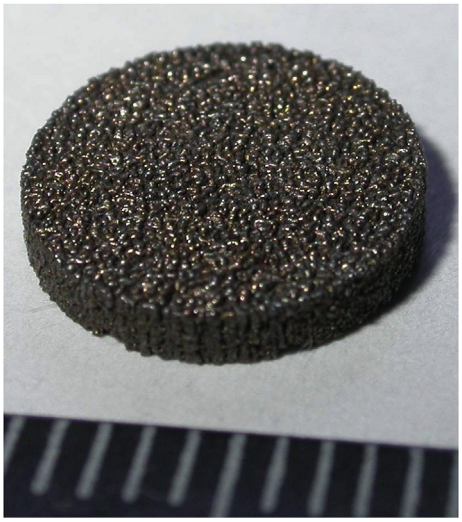

Fig. 4. Appearance of successful SLM sample. Disk with 10 mm in diameter. $P - 70$ W, $v - 140$ mm/s.

synthesis of $Cu_xAl_yNi_z$ intermetallic phase with complex stoichiometry. Dark inclusions are seen also (Fig. 5, S2 area) and are a result of the Cu_9Al_4 intermetallic phase quenching.

We made XRD patterns of synthesized after the SLM structures, the results are submitted in the Fig. 6. In the right upper corner XRD patterns conducted in study [8] are presented for the comparison. It is possible to confirm that synthesis of the rhombohedral Al_7Cu_4Ni intermetallic phase (28-0016, PDF2) with space group R-3m really took place under laser controlled SHS process. In particular, the intensity lines (111) and (115) are clearly seen, in our case they have duplex type. Lines of similar intensity were observed for the Al_7Cu_4Ni intermetallic phase in Ref. [27]. Indeed, after the restriction of the above EDS data, our XRD and EDS data are in a good agreement. We can conclude therefore that we have really obtained the Al7Cu4Ni intermetallide with slightly changed lattice parameters.

It is known that the electrical resistivity (ER) test provides more detailed information on the transformation occurring on the grain and crystalline levels. The ER method permits to study the phase transformations in metallic systems, to define the composition of different metallic mixtures, to conduct quantitative analysis of the phases in a solid solution [13,23].

The ER versus temperature curves during cooling and heating in the temperature range from −150 °C to +200 °C are shown in Fig. 7. In this figure, each dependence (two curves) consists of two parts. The heating stage of the porous CuAlNi sample from −150 °C up to +200 °C is given in red color and the cooling stage from +200 °C down to −150 °C in blue color. As it was mentioned in Refs. [13,23], a peak must appear during heating on the specific ER curve within the range of austenite transformation. Under cooling, a similar peak corresponds to the martensite transformation from a high-temperature phase for the CuAlNi in a low-temperature phase. In this case, the SME can be expected to develop in the CuAlNi sample.

Table 1
EDS date by SEM image (Fig. 5b).

Spectrum	Al	Ni	Cu
S1-all	53.40	4.75	41.85
S2	90.49	–	9.51
S3	41.07	5.92	53.01
S4	40.01	6.26	53.73

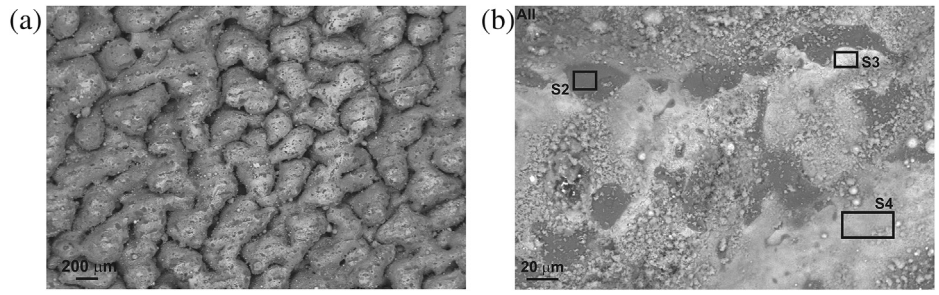

Fig. 5. Backscattering mode SEM images under different magnification: a) ×70, b) ×1000 with All (S1), S2–S4 EDS areas of elemental analysis.

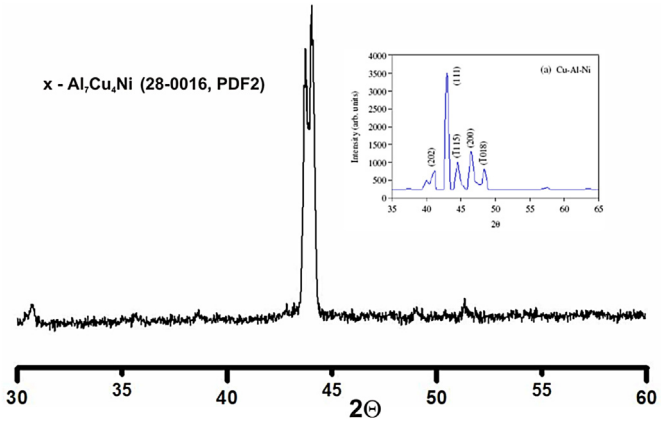

Fig. 6. XRD diffraction pattern of the sample, synthesized by SLM.

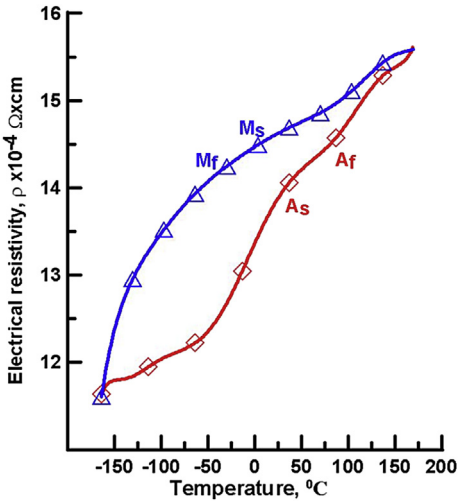

Fig. 7. Electrical resistivity of the CuAlNi synthesized by the SLM *vs.* temperature. LI parameters: $P = 70$ W, $D = 70$ μm, $Sh = 80$ μm, $v = 140$ cm/s.

Porosity of the CuAlNi leads to a peak shifting by the temperature axis, and the transformation temperature range broadens to the low temperature zone as well. Papers [13–15] showed a similar dependence of temperature at DSC peaks due to the phase transformations. One can see in Fig. 7 that the intervals of the austenite and martensite transformations are significantly displaced and broadened in the case of synthesized porous CuAlNi phase in contrast to cast CuAlNi [8,13–15]. Apparently, the interval of the A_s–A_f austenite transformation is 50 ÷ 80 °C, and the interval of the M_s–M_f martensite transformation is +25 ÷ −40 °C. The study [23] showed that the variation of Ni content by 0.1 at% changes the transformation temperature on approximately 10 °C, the presence of 1.0 at% oxygen decreases the martensite transformation temperature on 92.6 K and makes the parent phase brittle in the NiTi SMA. Obviously, similar effects could be observed in our case also.

4. Conclusion

For the first time the intermetallic CuAlNi samples were obtained by the two zone SLM process with the hatch distance of 80 μm, the laser power of 70 W, the laser beam diameter of 70 μm and with scan velocities 140 mm/s. It is shown that the SLM process implementation in argon has tendency to form the heterogeneous intermetallic phase of the rhombohedral Al_7Cu_4Ni type. The SEM with EDX analysis ensured about uncontrolled oxidation of Al. Evolution of the specific ER of porous CuAlNi samples synthesized by the SLS/SLM as a function of laser process parameters was experimentally studied.

Obviously, the ER measurement has proved to be a good method for identification of various phases and the SME in the porous Cu–Al–Ni SMA. The method proposed allows determining a temperature interval where the SME may be expected. Porosity of the CuAlNi leads to a peak shifting by the temperature axis and the interval of the A_s–A_f austenite transformation was 50 ÷ 80 °C, and the interval of M_s–M_f martensite transformation was +25 ÷ −40 °C.

The ER can be used as a feedback generator for controlling directly the location of the actuator with no need for other sensors. Owing to the SME in porous Cu–Al–Ni layer-by-layer synthesized by the SLS/M along with the possibility to manufacture 3D objects such as bio-MEMS–sensors, drug delivery systems, implants, etc., a new quality level can be achieved in orthopedic surgery by developing self-initiating, self-fixing, and self-swinging prosthetic elements at human body temperature.

Acknowledgments

The authors are grateful Prof. Smurov I. (director of DIPI, ENISE and LIAT, Stankin – mega grant 11.G34.31.0077) for the organizational support. Shishkovsky I. is separately grateful for financial support to the Russian Foundation of Basis Researches (grant 14-29-10193 ofi-m). Morozov Iu. is separately grateful for financial support to the Russian Foundation of Basis Researches (grant 13-03-12407 ofi-m2).

References

[1] I.V. Shishkovsky, M.V. Kuznetsov, Y.G. Morozov, I.P. Parkin, Laser-induced combustion synthesis of 3D functional materials: computer-aided design, J. Mater. Chem. 14 (2004) 3444–3448.
[2] I.V. Shishkovskii, A.G. Makarenko, A.L. Petrov, Conditions for SHS of intermetallic compounds with selective laser sintering of powdered compositions, Combust. Explos. Shock Waves 35 (1999) 166–170.

[3] J.H. Oh, S. Kirihara, Y. Miyamoto, K. Matsuura, M. Kudoh, Process control of reactive rapid prototyping for nickel aluminides, Mater. Sci. Eng. A 334 (2002) 120–126.
[4] L. Qin, J. Hu, C. Cui, H. Wang, Z. Guo, Effect of Al content on reaction laser sintering of Ni–Al powder, J. Alloys Compd. 473 (2009) 227–230.
[5] A.V. Kamashev, A.S. Panin, A.L. Petrov, I.V. Shishkovskii, Laser-controlled synthesis of nickel-aluminum intermetallic compounds, Tech. Phys. Lett. 27 (2001) 498–499.
[6] Y.H. Liu, Z.X. Guo, P. Shen, H.Y. Wang, J.D. Hu, Study on densification of laser ignited reaction sintering of Ni-Al-Cu powder, Sci. Sinter. 39 (2007) 31–37.
[7] T.M. Yue, T. Li, X. Lin, Microstructure and phase evolution in laser cladding of Ni/Cu/Al multilayer on magnesium substrates, Metall. Mater. Trans. A 41 (2010) 212–223.
[8] V. Sampath, Studies on the effect of grain refinement and thermal processing on shape memory characteristics of Cu–Al–Ni alloys, Smart Mater. Struct. 14 (2005) S253.
[9] M. Čolić, R. Rudolf, D. Stamenković, I. Anžel, D. Vučević, M. Jenko, V. Lazić, G. Lojen, Relationship between microstructure, cytotoxicity and corrosion properties of a Cu–Al–Ni shape memory alloy, Acta Biomater. 6 (2010) 308–317.
[10] S.P. Kuruvilla, C.S. Menon, Third-order elastic constants and low-temperature thermal expansion of the shape memory alloy Cu–Al–Ni, Smart Mater. Struct. 15 (2006) 1974.
[11] P. Blanc, C. Lexcellent, Micromechanical modelling of a CuAlNi shape memory alloy behaviour, Mater. Sci. Eng. A 378 (2004) 465–469.
[12] V. Recarte, V. Sánchez-Alarcos, J.I. Pérez-Landazábal, Influence on the martensitic transformation of the β–phase decomposition process in a Cu-Al-Ni shape memory alloy, J. Phys. Condens. Matter 17 (2005) 4223–4236.
[13] I.V. Shishkovsky, Shape memory effect in porous volume NiTi articles fabricated by selective laser sintering, Tech. Phys. Lett. 31 (2005) 186–188.
[14] R. Löbel, S. Thienhaus, A. Savan, A. Ludwig, Combinatorial fabrication and high-throughput characterization of a Ti–Ni–Cu shape memory thin film composition spread, Mater. Sci. Eng. A 481–482 (2008) 151–155.
[15] P.-A. Gédouin, S.A. Chirani, S. Calloch, Phase proportioning in CuAlBe shape memory alloys during thermomechanical loadings using electric resistance variation, Int. J. Plast. 26 (2010) 258–272.
[16] Y. Aydogdu, A. Aydogdu, O. Adiguzel, Self-accommodating martensite plate variants in shape memory CuAlNi alloys, J. Mater. Process. Technol. 123 (2002) 498–500.
[17] G. Lojen, I. Anžel, A. Kneissl, A. Križman, E. Unterweger, B. Kosec, M. Bizjak, Microstructure of rapidly solidified Cu–Al–Ni shape memory alloy ribbons, J. Mater. Process. Technol. 162–163 (2005) 220–229.
[18] C. Picornell, V.A. L'vov, J. Pons, E. Cesari, Experimental and theoretical study of mechanical stabilization of martensite in Cu–Al–Ni single crystals, Mater. Sci. Eng. A 438–440 (2006) 730–733.
[19] U. Sarı, İ. Aksoy, Micro-structural analysis of self-accommodating martensites in Cu–11.92 wt%Al–3.78 wt%Ni shape memory alloy, J. Mater. Process. Technol. 195 (2008) 72–76.
[20] N. Suresh, U. Ramamurty, Aging response and its effect on the functional properties of Cu–Al–Ni shape memory alloys, J. Alloys Compd. 449 (2008) 113–118.
[21] I. Yadroitsev, Selective Laser Melting: Direct Manufacturing of 3D-objects by Selective Laser Melting of Metal Powders, LAP Lambert Academic Publishing AG & Co KG, 2009, p. 280.
[22] E.M. Mazzer, C.S. Kiminami, P. Gargarella, R.D. Cava, L.A. Basilio, C. Bolfarini, W.J. Botta, J. Eckert, T. Gustmann, S. Pauly, Atomization and selective laser melting of a Cu-Al-Ni-Mn shape memory alloy, Mater. Sci. Forum 802 (2014) 343–348.
[23] I.V. Shishkovsky, Simulation of thermomechanical and electrothermal hysteresis phenomena in porous nickel titanium, Tech. Phys. 59 (2014) 297–303.
[24] I.V. Shishkovsky, V.I. Scherbakov, Y.G. Morozov, M.V. Kuznetsov, I.P. Parkin, Surface laser sintering of exothermic powder compositions, J. Therm. Anal. Calorim. 91 (2008) 427–436.
[25] I.V. Shishkovskiy, Y.G. Morozov, M.V. Kuznetsov, I.P. Parkin, Electromotive force measurements in the combustion wave front during layer-by-layer surface laser sintering of exothermic powder compositions, Phys. Chem. Chem. Phys. 11 (2009) 3503–3508.
[26] S.E. Zakiev, L.P. Kholpanov, I.V. Shishkovsky, I.P. Parkin, M.V. Kuznetsov, Y.G. Morozov, Modelling of the thermal processes that occur during laser sintering of reacting powder compositions, Appl. Phys. A 84 (2006) 123–129.
[27] R. Herrera, O. Soriano, H.J. Dorantes, V.M. López, Caracterización microestructural del compuesto intermetálico Al7Cu4Ni, Rev. Metall. 40 (2004) 118–121.